Korea Polymer Journal, Vol. 8, No. 3, pp 103 – 115 (2000)

Korea Polymer Journal

Volume 8, Number 3 June 30, 2000

Crystallization Behavior of Polymers as Viewed from the Molecular Level

Kohji Tashiro*, Sono Sasaki, Yoko Ueno, Akiko Yoshioka, and Masamichi Kobayashi

Graduate School of Science, Osaka University, Toyonaka, Osaka 560-0043, Japan

Received February 7, 2000

Abstract : The structural changes viewed from the molecular level have been investigated for the isothermal crystallization phenomena of polyethylene (PE) and the solvent-induced crystallization phenomenon of syndiotactic polystyrene (sPS) glassy sample.The data, which were collected by the time-resolved measurements of Fourier-transform infrared spectra, Raman spectra, synchrotron-sourced small-angle X-ray scattering, wide-angle X-ray scattering, and so on, were combined together to extract the detailed structural information in these phase transition phenomena. In the case of PE, the isothermal crystallization from the melt to the orthorhombic form was found to occur via the conformationally-disordered trans chain form, followed by the formation of the lamellar stacking structure of regular orthorhombic-type crystals. In the case of sPS, the amorphous chains in the glassy sample were found to enhance the mobility through the interaction with the injected solvent molecules, which act as a trigger to cause the conformational ordering from the random coil to the regular T_2G_2-type helical form. The thus created short helical segments were found to grow into longer helices, which gathered together to form the crystallites, as revealed by the organized coupling of the infrared, Raman and X-ray scattering data.

General Introduction

In general, the crystalline polymers exhibit the so-called higher-order structure built up by the complicated combinations of the crystalline, amorphous and intermediate regions. Clarification of the details of this higher-order structure may give us useful leading principles necessary for the development of new polymer materials with excellent physical properties. For this purpose, however, it may be also important to clarify the formation mechanism of such a structure from the

*e-mail : ktashiro@chem.sci.osaka-u.ac.jp

molecular level. Let us consider the case of polyethylene as an example. Polyethylene is melted at high temperature and slowly cooled to the room temperature. In the melt the molecular chains are considered to take the shape of random coils. Below the crystallization temperature, the spherulites are formed, in which the lamellae are stacked together and grow in the radial direction. In one lamella many molecular chains are aggregated to form the crystalline lattice with folding structure on the surfaces of the lamella. How are the lamellae formed from the random coils in the process of crystallization? The phenomenological investigations were made by many researchers. But, in order to understand the essential features of the crystallization mechanism, the detailed structural changes in the crystallization process should be clarified from the microscopic point of view.

In these studies the structure and its transformation process must be viewed from the various directions by an organized combination of the various kinds of the experimental methods such as the wide-angle X-ray scattering (WAXS), small-angle X-ray scattering (SAXS), Fourier-transform infrared spectra, Raman spectra, etc. In this paper these different methodologies will be applied to the following two themes of crystallization phenomena: (1) isothermal crystallization of polyethylene (PE) from the melt and (2) solvent-induced crystallization of syndiotactic polystyrene (sPS) from the glassy state.

1. Isothermal Crystallization of Polyethylene from the Melt

The structural change during the isothermal crystallization of PE has been investigated extensively from the view points of lamellae and spherulite.[1-12] However these studies are concerned mainly with the mechanism of the nucleation and growth of crystallites at the lamellar level by utilizing the small-angle X-ray (SAXS) and light scattering (SALS) techniques. But the structural information about the conformational ordering of the molecular chains could not be obtained at all, which should be quite important in the clarification of the essential features of the crystallization mechanism. For this purpose the vibrational spectroscopy is one of the most powerful methods. We carried out the time-resolved measurements of the FTIR and SAXS in the course of the isothermal crystallization of PE, and observed the crystallization behavior from both the microscopic and macroscopic points of view by organized combination of these two different types of the data.[13-15]

1-1. Vibrational Bands Characteristic of Various Molecular Conformations.

In order to clarify the conformational changes in the isothermal crystallization phenomenon by vibrational spectroscopy, an information on the infrared (and Raman) bands characteristic of the various conformations is needed. The PE crystal is known to experience the transition between the orthorhombic and hexagonal phases by applying high temperature and high pressure[16,17] or by applying high tensile stress along the chain direction immediately below the melting point.[18-21] The molecular chains in the hexagonal phase are speculated to take the disordered conformation consisting of long trans segments interrupted by an invasion of gauche bonds. This speculation was made on the basis of the molecular dynamics calculation[22] but had not been confirmed experimentally. Then we measured the spectral changes in the phase transitions between the orthorhombic, hexagonal and liquid phases in order to extract the information on the molecular conformations.[23]

The infrared spectra of the hexagonal phase were measured by heating the ultra-drawn PE fiber, the ends of which were tightly bound to get the high tensile stress along the fiber axis. For example, Figure 1 shows the X-ray diffraction patterns taken by a two-dimensional imaging plate detector for the ultra-drawn PE fiber in the heating process (the heating rate 0.7 °C/min).[23] As the temperature was increased to the phase transition region which was detected by the DSC measurement, the intensity of the 110 and 200 reflections of the orthorhombic phase was decreased and the 100 reflection of the hexagonal phase began to appear. With further increase of the temperature, the orthorhombic phase disappeared finally and the hexagonal phase increased its intensity. In higher temperature region, the reflection pattern

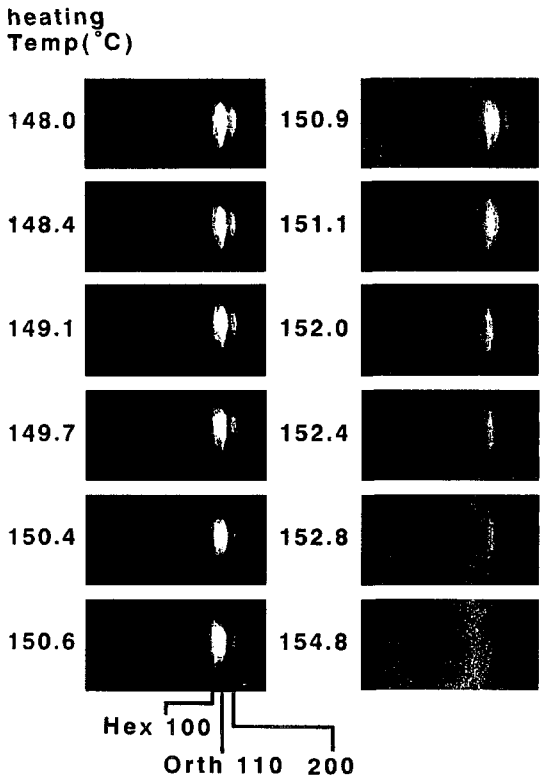

Figure 1. Temperature dependence of the X-ray diffraction pattern measured for the constrained PE sample in the heating process by the DIP220 imaging plate system. Orth : the orthorhombic phase, and Hex : the hexagonal phase.

changed to the halo characteristic of the molten state. By analyzing the temperature dependence of the integrated intensity of the reflections, the transition between the orthorhombic and hexagonal phases could be detected clearly around 146-154°C. Along this phase transition detected by the X-ray diffraction measurement, the IR spectra were measured for the constrained sample, where the ultra-drawn film was wound tightly many times around the KBr holder. For the strain-free sample, the film was sandwiched between a pair of KBr plates. The infrared spectral change in the frequency regions of the CH_2 bending and rocking modes is shown in Figure 2. For example, in the CH_2 bending region, the new bands appeared around 1460-1470 cm^{-1} and increased the intensity remarkably, while the intensity of the orthorhombic crystalline band (1471 cm^{-1}) was decreased. In higher temperature region, the intensity of these new bands decreased and the amorphous bands were observed intensely. The infrared bands of similar behavior were observed also in the CH_2 rocking and wagging regions, which showed clear polarization characters. The behavior of these infrared bands are very similar to those observed in the orthorhombic-to-hexagonal transition of *n*-alkane crystal, in which the bands characteristic of the disordered chain conformations such as ..TTGTG̅TT.. and ..TTGGTT.. were assigned.[24,25]

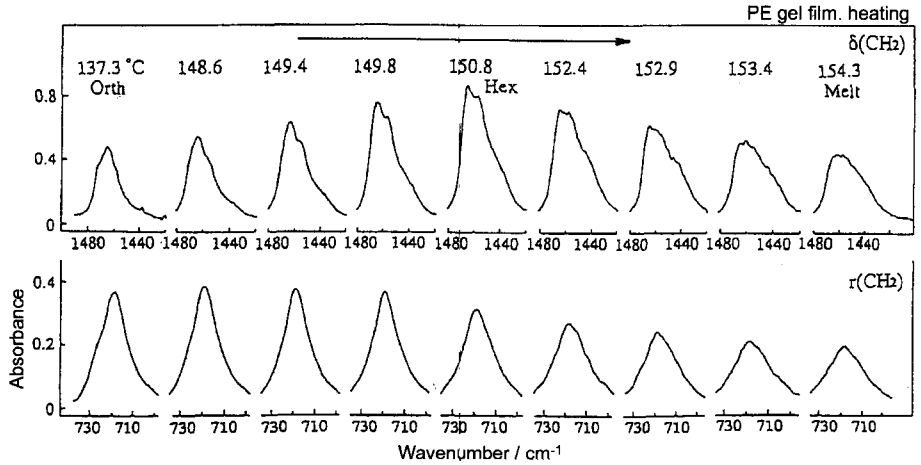

Figure 2. The infrared spectral change in the frequency region of the (upper) CH_2 bending modes and (lower) CH_2 rocking modes measured for the constrained PE film in the heating process.

From these analyses, including the curve separation process, we have been able to identify the bands characteristic of the conformationally-disordered hexagonal phase of PE. The main bands are listed as below.

1466, 719 cm^{-1}	disordered trans segments
1366, 1306 cm^{-1}	kink (..TTGTG$\bar{T}$TT..)
1352 cm^{-1}	double gauche (..TTGGTT..)

1-2. Time-Resolved Infrared Measurement in the Isothermal Crystallization.

As stated above, the IR bands characteristic of the hexagonal phase or the conformationally-disordered (CONDIS) phase were revealed. By referring to these spectral information, we made the time-resolved FTIR measurements in order to clarify the structural changes during the isothermal crystallization process of PE samples.[13] In the isothermal crystallization experiments, it is quite important to cool the samples as fast as possible from the molten state to T_c or the crystallization temperature. Besides the T_c should be kept constant and stable. Therefore, the temperature-jump apparatus was designed carefully for the time-resolved FTIR measurement. The cooling rate was 600-4200°C/min. In order to measure the sample temperature, the thermocouple was embedded "into" the sample and the temperature change was directly recorded by an x-y recorder. After the jump was completed the temperature was stabilized with sufficiently small fluctuation (ca.±0.2 °C at maximum). FTIR spectra were measured by a Bio-Rad FTS-60A/896 Fourier-Transform infrared spectrometer equipped with an MCT detector in the rapid scan mode at a rate of 0.3-1.0 sec/spectrum with the resolution power of 2 cm^{-1}.

As for the samples, a high-density PE (HDPE) and a linear low-density PE (LLDPE) were used. The characterization of these samples was made as follows.

	M_w	M_n	M_w/M_n	ethyl branching/ 1000C
HDPE	126K	24K	5.3	1
LLDPE	75K	37K	2.0	17

The LLDPE sample was used here because the crystallization rate could be reduced more easily than HDPE while keeping the essentially same crystallization behavior as that of HDPE.

Figure 3 shows the IR spectra picked up from a series of spectra taken for the LLDPE sample during the isothermal crystallization from the melt at the degree of supercooling $\Delta T = 4$ °C, where the time indicated in this figure was measured from the starting point ($t = 0$), which was defined as the time when the temperature reached just the predetermined crystallization point (T_c). The ΔT is defined originally as $T^\circ_m - T_c$ (T°_m: the equilibrium melting temperature), but, because of the practical reasons, it was defined here as $T^\circ_c - T_c$ where T°_c was the temperature at which the crystallization began to be observed in the non-isothermal slow crystallization experiment (T°_c for HDPE and LLDPE were 123 and 109 °C, respectively). The three spectra in Figure 3 are assumed respectively to be characteristic of (a) the melt (including some effect from the intermediate state already), (b) the intermediate state, and (c) the orthorhombic crystal (at high temperature or with low degree of crystallinity). The spectra of the intermediate state are different from those of the melt and the

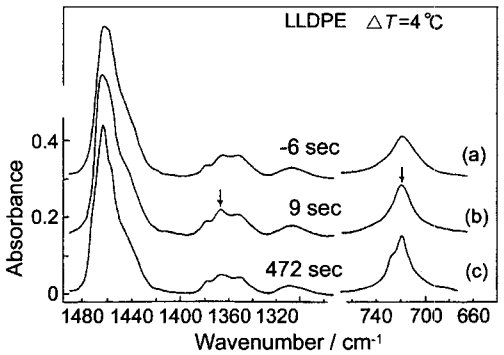

Figure 3. FTIR spectra of LLDPE sample, extracted from a series of spectra measured at constant time interval during the isothermal crystallization from the melt at ΔT= 4 °C and cooling rate of ca. 600 °C/min.(a), (b) and (c) correspond to the spectra of the melt, the intermediate state (disordered trans form) and the orthorhombic crystal, respectively, although an overlapping of the spectra between the different states must be considered more or less. The bands pointed by arrows in (b) correspond to the disordered trans form discussed in the text.

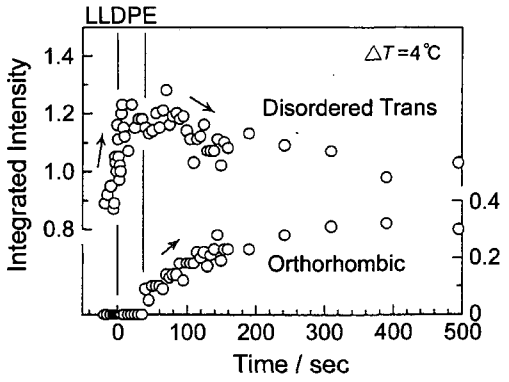

Figure 4. Time dependence of the integrated intensity of IR bands measured for LLDPE during the isothermal cry- stallization from the melt at ΔT=4 °C and cooling rate of ca. 600 °C/min.The vibrational frequency of the analyzed disordered-trans band is 1368 cm^{-1} and that of the ortho- rhombic phase is 728 cm^{-1}.

orthorhombic crystal. The bands detected in the intermediate state correspond to the disordered trans bands characteristic of the CONDIS phase mentioned in the preceding section. That is to say, at the beginning of the isothermal crystallization, the bands characteristic of the melt decreased in intensity and the bands corresponding to the disordered trans form increased in intensity. After that the exchange of intensity began to occur between the bands of disordered trans form and the bands intrinsic to the long and regular trans segments (the orthorhombic crystalline bands) at 1471 and 728 cm^{-1}. As an example, the time dependence of the intensity of the disordered trans band at 1368 cm^{-1} is plotted in Figure 4. The band began to increase its intensity during the temperature jump and kept increasing it even after the temperature reached the T_c. After keeping at maximum for a while, this band intensity began to decrease gradually. In this time region, the long and regular trans band at 728 cm^{-1} appeared and increased in intensity. This type of observation could be made also for the different degrees of supercooling and for the HDPE sample. From all the data obtained in the temperature jump experiments, it was concluded that the chain conformational change occurs from the random coil to the regular planar-zigzag form via the disordered trans-form in isothermal crystallization from the melt.

1-3. Time-Resolved SAXS Measurement in the Isothermal Crystallization.

So far the conformational ordering of chains was discussed. It is important to clarify the relation of this conformational change with the change in the aggregation structure of lamellae in order to understand the details of the isothermal crystallization mechanism. Therefore, in parallel to the infrared spectral measurement, we carried out also the time-resolved SAXS measurements during isothermal crystallization of the various PE samples at almost the same temperature jump rate of 600 °C/min.[14] The SAXS measurements were performed in the Photon Factory, National Laboratory for High Energy Physics, Tsukuba, Ibaraki, Japan (the wavelength of the incident X-ray beam λ=1.4881 Å and the sample-to-detector distance 1900 mm). The scattered X-ray signal was detected by using a one-dimensional position sensitive proportional counter (PSPC) for the collection time of 3-7 sec and at a time interval of 3-7 sec. The time dependence of the SAXS profiles measured for LLDPE sample during the isothermal crystallization at ΔT=4 °C is shown in Figure 5 (In order to make the characteristic features clearer, the case of fully-deuterated high-density PE (DHDPE) is also reproduced here). These profile changes may be divided into three stages of time evolution.

Time Region I (t=0~100 sec) : After the sample was cooled rapidly to T_c from the melt, a Lorentzian-type SAXS profile appeared, whose peak was expected to be positioned at q=0 $Å^{-1}$ and increased its intensity [the wave vector q is equal to $(4\pi/\lambda)\sin\theta$ (θ:Bragg angle)]. We assumed that this profile change may be interpreted on the basis of the density-fluctuation in the homogeneous system. In this case the scattering intensity $I(q)$ should follow the Ornstein-Zernike (O-Z) equation, $1/I(q)=[1/I(0)]\ [1+q^2\xi^2]$, where $I(q)$ is the scattering intensity at q and ξ is the correlation length. In fact, a good linear relation could be obtained between $1/I(q)$ and q^2 for the data of Figure 5, indicating an occurrence of the density fluctuation in the homogeneous molten state.

Time Region II (t=100~220 sec) : In this time region, a peak began to be detected at ca. q =0.008 $Å^{-1}$ and increased its intensity with time,

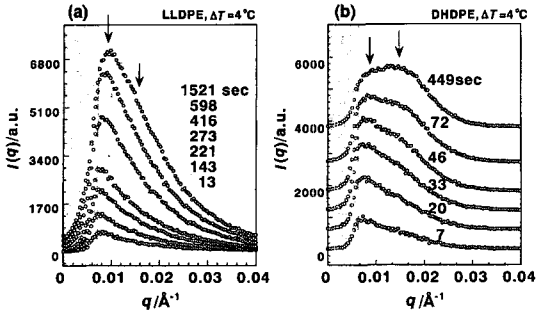

Figure 5. Time dependence of the SAXS profiles measured for (a) LLDPE and (b) DHDPE samples at the supercooling $\Delta T=4$ °C in the isothermal crystallization process from the melt(Figures' Caption continued 1).

implying an appearance of a periodic structure of 700-800 Å. The $I(q)$ at a constant q position was found to be expressed by an exponential function of time; $I(q) \propto \exp[k \cdot t]$. This behavior of $I(q)$ is apparently similar to the spinodal decomposition observed for polymer alloy.[26] But, in general, the concept of spinodal decomposition is applied to the case where the so-called conservation law is held in the system. The observation of the long period at $q=0.008$ Å^{-1} suggests the drastic change in the order parameter necessary for the description of the structural transition in the crystallization process (or non-conservation of the order parameter before and after the transition). That is to say, the observation of the long period does not seem to match the concept of spinodal decomposition in this time region. Rather, it might be reasonable to assume an occurrence of nucleation and growth of the crystalline lamellae in the time region II.

Time Region III ($t=220$ sec~) : As the time passed furthermore, a new phenomenon was observed. That is, a shoulder began to appear around $q=0.016$ Å^{-1} and its intensity gradually increased. At the same time the original peak of 800 Å period reduced the increasing rate (or decreased gradually). This new peak corresponds to the periodical structure of ca. 400 Å. In this way the periodic structure of about 800 Å changed gradually into the periodic structure of 400 Å in the crystallization of PE, indicating that a new lamella is generated between the already existing lamellae of 800 Å period and the lamellar stacking structure takes ca. 400 Å period.

1-4. Structural Changes Viewed from the Coupled Data of FTIR and SAXS.

The temperature jump was carried out at almost the same rate of ca. 600°C/min in both the measurements of FTIR and SAXS. Then, as shown in Figure 6, the time dependence of the structural parameters of lamella, which is obtained by the calculation of the correlation function from the SAXS data, is compared with that of the IR band intensities estimated for LLDPE at $\Delta T=4$ °C. From this comparison we may draw the structural change in the crystallization process

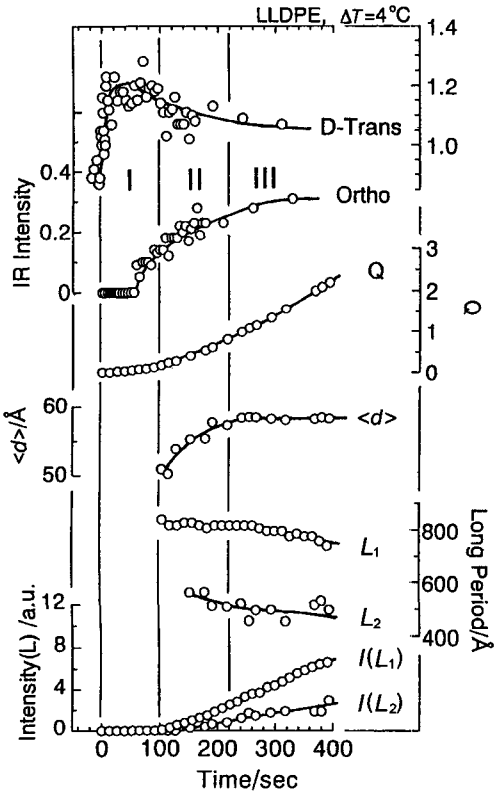

Figure 6. Combination of the vibrational spectroscopic data with the SAXS data collected for the LLDPE sample in the isothermal crystallization process from the melt at $\Delta T=4$ °C. Q: invariant evaluated from the total integration of the observed SAXS profile, $<d>$: lamellar thickness. L_1(800 Å) and L_2(400 Å) denote, respectively, the long spacings of the lamellar stacking structure. $I(L_1)$ and $I(L_2)$ denote the intensities measured for the SAXS peaks corresponding to these periods.

concretely.[13-15]

Before this structural change is described, however, we have to talk about the aggregation state of the chains in the melt as well as in the lamella. We carried out the small- and wide-angle neutron scattering (SANS and WANS) experiments, the thermal analysis and the infrared spectral measurements for a series of blend samples between the fully-deuterated high-density PE (DHDPE) and the hydrogeneous LLDPE used in the above experiments.[15] All the experimental data obtained for these samples may be summarized in the following ways. (1) For each sample only one melting peak is observed in the DSC thermogram, which shifts continuously with the D/H content.[27] (2) The infrared band profiles in the methylene bending- and rocking-mode regions change systematically between the doublet to the singlet depending on the D/H content. (3) The SANS data gave us the information that the homogeneous (or random) mixing of the D and H chains can be seen in both the molten state and the crystalline state of the D/H blend samples. (4) According to the SANS data analysis, the radii of gyration (R_g) of the D and H chains do not change before and after crystallization from the melt. (5) The broad scattering is observed in the low angle region of the WANS pattern for the slowly-cooled D/H blend sample as well as for the molten state. All the experimental results of (1) to (5) could be interpreted theoretically on the basis of such a model that the D and H chains are statistically randomly packed in the *same* crystal lattice (i.e. the cocrystallization phenomenon).[15, 27] This idea of random arrangement of the chain stems in the crystalline lamella may be reasonably connected with the statement that the PE chains experience the random reentry folding on the surface of the crystalline lamella.

The experimental result (4) is important, which states that the radius of gyration of an individual chain is kept unchanged even when the chain is enrolled into the crystalline lamella from the melt. Thus, by combining all the experimental data mentioned so far, we may describe the structural changes occurring in the isothermal crystallization process of PE as shown in Figure 7.[15]

The molecular chains in the melt take the form of random coils. When the sample is cooled to the crystallization temperature, some parts of the chain segments change their conformation to the disordered trans form, just when the total size of the chain is not changed in average (Time Region I). The chains are entangled with each other but the disordered trans segments of these entangled parts are gathered together to form a single lamella by arranging themselves side by side, just when the molecular chain segments change the conformation to more regular trans-zigzag form (Time Region II). As a result, the chain folding of random reentry type is realized. The total size of the chain is still unchanged. These lamellae are stacked together with the long period of ca. 800 Å. With the pa-ssage of time, the 800 Å periodical structure changes to the structure with a long period of ca. 400 Å, indicating that new lamellae are created in between the already existing lamellae and the more densely stacked lamellar structure is constructed (Time Region III).

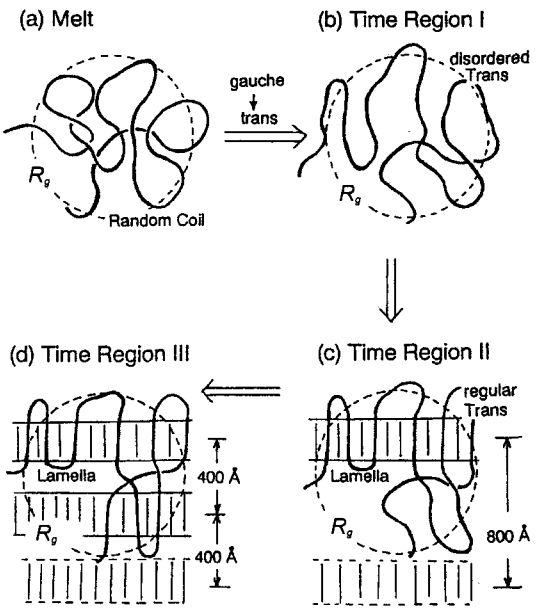

Figure 7. Illustrated structural change in the crystallization process of PE from the melt. The segments of the random coils change to the regular zigzag conformation *via* the disordered trans form. In this course of disorder-to-order transition of the chains, the formation and stacking of lamellae occur. It should be noted that the radius of gyration of the chain is not changed in this process.

2. Solvent-induced Crystallization of Syndiotactic Polystyrene.

Syndiotactic polystyrene (sPS) takes two types of molecular conformations in the crystalline region. Roughly speaking, random coils of the glassy state regularize to the planar zigzag form by annealing and to a complex of T_2G_2 form by absorption of organic solvents.This T_2G_2-solvent complex transfers to the planar zigzag form by removal of the guest solvent by heating. These changes remarkably depend on the thermal history of the samples, the kind of solvent, and so on.[30-50] Although a number of studies were made to analyze the structure of these crystalline forms very little has been clarified about the phase transition behavior of the complicated polymorphs of sPS. In the second part of this paper we will trace the solvent-induced crystallization of the glass by comparing the experimental data obtained by the various types of the time-resolved measurements such as IR, Raman, and wide-angle X-ray scattering.[51-53] For the solvent we will focus our attention only to the case of toluene, as an example.

2-1. Time-Resolved IR & Raman Spectral Measurements. The glassy sPS samples were prepared by quenching the molten films to the liquid nitrogen. The sample was set into the optical cell with the solvent reservoir. The infrared or Raman measurement was started at the same time with the solvent injection into the reservoir. The infrared spectra were recorded at a constant interval of about 2 seconds at a resolution power 2 cm^{-1} by using a Bio-Rad FTS-60A FT-IR spectrometer equipped with an MCT detector. The Raman spectra were measured by using a Japan Spectroscopic Company NR1800 dispersion-type Raman spectrometer with a CCD detector. The wavelength of the excitation light was 514.5 nm, which was taken from Ar-ion laser with a power of 48 mW. Each Raman spectrum was collected for every 80 sec at a time interval of 10 sec. The resolution power was 2 cm^{-1}.

Figures 8 and 9 show, respectively, the time dependencies of IR and Raman spectra taken for the sPS-toluene system. For example, in Figure 8, we can recognize the appearance and evolution

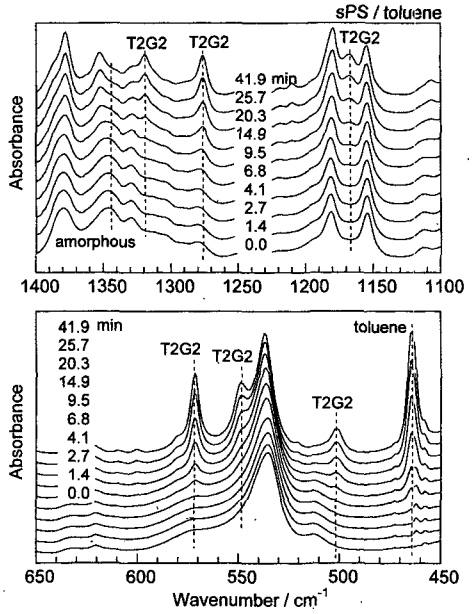

Figure 8. Time evolution of FTIR spectra measured for the sPS glass film exposed to toluene vapour at room temperature. The time shown in this figure was measured from the moment of injection of the solvent.

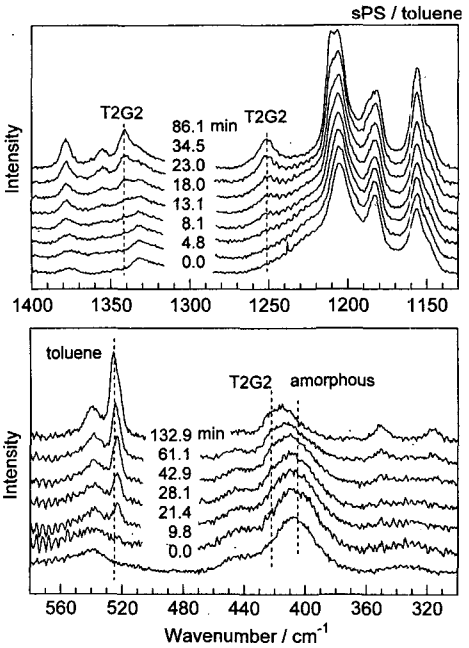

Figure 9. Time evolution of Raman spectra measured for the sPS glass film exposed to toluene vapour at room temperature. The time shown in this figure was measured from the moment of injection of the solvent.

of the crystalline bands and the intensity decrement of the amorphous bands immediately after the injection of solvent. The similar situation can be also seen in the Raman spectra shown in Figure 9. When the integrated intensities of the bands, which were evaluated after curve separation, are plotted against time, the timing of the appearance is noticed to be different among the bands. Immediately after the solvent injection, the intensity of the toluene band increased. This was followed by the decrease of the intensity of the amorphous band and the intensity increase of the T_2G_2 conformation bands at 549 cm^{-1} etc. After that, the intensity of the T_2G_2 bands at 1251, 572 cm^{-1}, etc. began to increase. This difference in timing of the bands is considered to come from the difference in the so-called critical sequence length. That is to say, the crystalline-sensitive bands have the characteristic critical sequence length (m) and do not appear until the chain length of regular conformation exceeds the m.[54, 55] The m can be evaluated on the basis of the intramolecular isotope-dilution technique.

In this method, the random copolymers of the hydrogeneous (H) and deuterated (D) monomers with various compositions are used and the IR (and/or Raman) spectra are measured. The H monomer sequence is cut by an invasion of the D monomeric units and the vibrational wave propagating over the H monomer sequence is interrupted, resulting in the decrement of the band intensity. The band intensity is related with the averaged length of the H sequence or the molar content of the H species and can be expressed by a theoretical equation as a function of the H content. Therefore, by fitting the theoretical curve with the observed data collected for a series of the H/D copolymers, we can determine the m of this band. For example,the Raman band at 243 cm^{-1} was found to have the m of 2-5. That is to say, this band can be detected in the Raman spectra for the first time when 2-5 monomers are arranged into a regular helix conformation. In the case of the 1251 cm^{-1} Raman band, the m is 8-12; in other words, about 10 monomeric units must be incorporated into a regular conformation for the detection of this band, corresponding to about 2 repeating periods of the T_2G_2 helical chain or ca. 16 Å along the chain axis.

By taking into account these m values, we can describe the evolution of the regular helix conformation induced by the injection of toluene molecules as follows. Starting from the random coils in the amorphous region, they are regularized into the short helical form when the interaction is started between toluene molecules and the glassy chains. After that, these short helices grow to longer and more regular helical chains as detected by the intensity increase of the bands with high m values.

2-2. Time-Resolved X-ray Scattering Measurement.

The wide-angle X-ray scattering measurement was performed as a function of time by using an imaging plate system (DIP220, MAC Science, Japan). Starting from the glassy sample, the crystalline peaks could be observed when some time passed after injection of toluene solvent. The time evolution of the scattering intensity of the crystalline peak is compared with those of IR and Raman band intensities as shown in Figure 10 (In

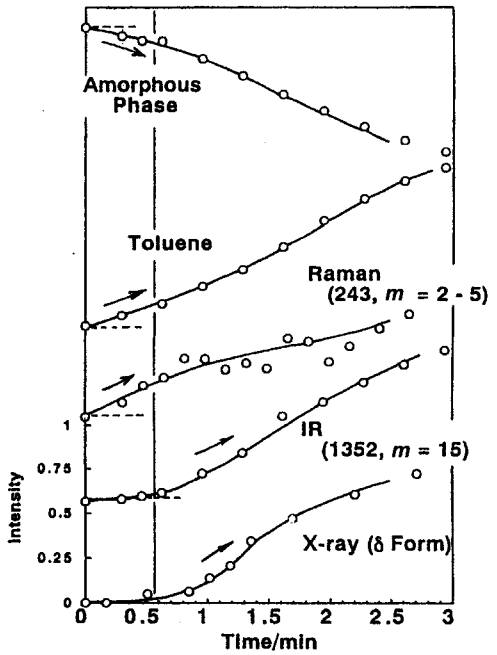

Figure 10. Time evolution of relative intensities of IR bands, Raman bands, and X-ray scattering measured for the glassy sPS sample exposed to the toluene vapor.

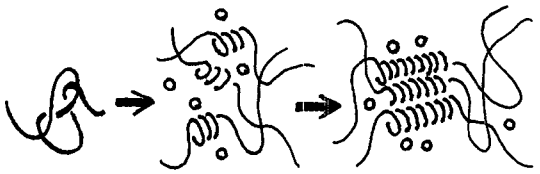

Figure 11. An illustration of solvent-induced structural ordering process of sPS glass sample.

this figure the intensities of the IR bands, Raman bands, and X-ray peaks originating from the amorphous region were unified to the same value because these data were collected independently by using the samples with different thickness or with the different time scale of transition). Immediately after the absorption of toluene, the random coils in the amorphous phase interacts with the toluene molecules and begin to regularize partly into the short T_2G_2 chain segments, as seen in the increase of the corresponding IR and Raman band intensity (m=2-5). After several times pass, the short helices grow to the longer helices, as judged from the appearance of the corresponding bands with higher m values. The X-ray scattering peaks characteristic of the crystalline phase are detected almost at the same timing with these IR and Raman bands, indicating the formation of some crystalline clusters by the aggregation of the long helical segments (see Figure 11).

2-3. Thermal Motion of the Amorphous Chains in the Induction Period of Crystallization.

The glass transition temperature (T_g) of sPS is about 100 °C, much higher than room temperature. In the general crystallization process of polymers, the heat treatment is made above T_g. As described above, the solvent-induced crystallization of sPS sample is induced even at room temperature, much lower than T_g. Therefore we may speculate reasonably that the motion of the molecular chains in the amorphous region is accelerated when the chains interact with the solvent molecules. In other words, the solvent is speculated to play a role of plasticizer to induce the crystallization of the amorphous phase. In order to prove this speculation experimentally, the molecular motion must be detected directly by any physicochemical method.

The solid-state NMR method might be one of the possible candidates. But the induction period is too short to be detected by this method. Besides, it is difficult to introduce the solvent into the rapidly spinning NMR sample tube. The measurement of dielectric dispersion spectra might be another candidate: the dielectric loss peak corresponding to the chan motion in the amorphous phase should be observed when the solvent is introduced into the sample. In this experiment the film surface must be contacted directly to the metal electrode, making an invasion of solvent vapor into the sample film difficult. The direct contact of the electrode is needed because of such a reason that the exact evaluation of the dielectric constant of the sample itself becomes very difficult when any small gap is present between the sample surface and the metal electrode, since the dielectric constant of solvent (and air) might be overwhelmingly larger than that of the sample. The dynamic viscoelastic measurement can be used, but the full filling of the solvent vapor in the large sample box is experimentally awful.

Then we got an idea to measure the change of the half-width of the infrared band intrinsic of the amorphous structure before and after the solvent injection.[52, 53] This is based on such an idea that the half-width of the band is a measure of the molecular motion and it is inversely proportional to the relaxation time of the motion of the groups associated with this vibrational band: the band is

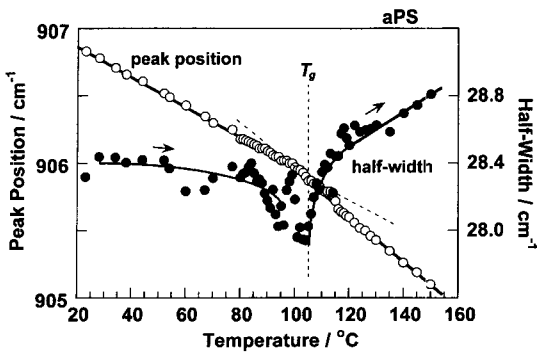

Figure 12. Temperature dependence of the half-width and peak position of the infrared band at 907 cm^{-1} measured for atactic PS sample.

broader as the motion is more vigorous or the relaxation time is shorter. In order to confirm the usefulness of this idea, we measured, as an example, the temperature dependence of the half-width of the infrared band of the amorphous atactic polystyrene (aPS) sample. Figure 12 shows the peak position and the half-width of the 907 cm^{-1} amorphous band of aPS measured in the heating process from room temperature. The half-width increased steeply above T_g, confirming our speculation reasonably. Besides the peak position of the band shifted to lower frequency side with the deflection point around T_g. Such type of the spectral change could be seen also for the amorphous band around 560 cm^{-1} and so on.

This technique was actually applied to the present case and the peak position and half-width of the amorphous bands of sPS were measured in the process of the solvent injection. The results are shown in Figure 13, where the integrated intensity of the crystalline bands is also plotted for comparison. The similar phenomenon can be observed more clearly for the case of benzene injection, as shown in Figure 14. Immediately after the injection of solvent into the glassy sPS film, the intensity of solvent bands started to increase and at the same time the half width of the amorphous band (at 565 cm^{-1}) began to increase. The peak position of this band was found to shift to lower frequency side. Around 2 minute after the solvent injection, the crystalline bands with short m (549 cm^{-1}, $m=2$-4) started to increase their intensities. The intensities of the crystalline bands with long m (572 cm^{-1}, $m=20$-30) increased a little later than the bands with short m. From these experimental data the following scheme may be extracted. After the injection of solvent, the amorphous chain interacts with the solvent and accelerates the mobility even below T_g. This chain motion works as a trigger to cause the conformational ordering to generate the short helical segments. As the process is advanced, the longer helical segments are grown, which aggregate together to form the crystalline lattice as illustrated in Figure 11. At this

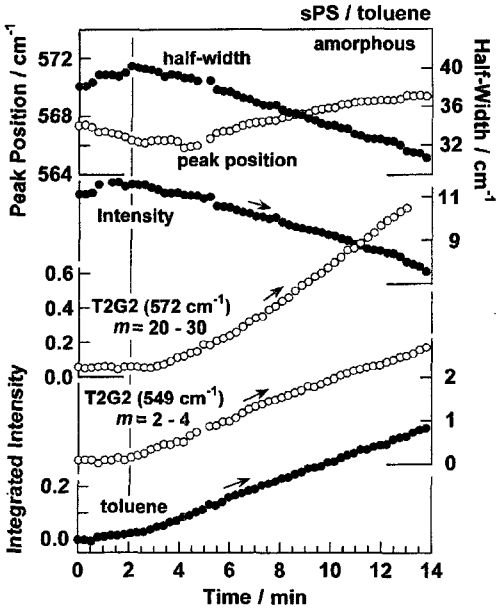

Figure 13. Time dependencies of the half-width, peak frequency, and integrated intensity of the 565 cm^{-1} amorphous band of the glassy sPS film measured in the process of toluene injection at room temperature, which are compared with the time dependencies of the integrated intensities of the crystalline-sensitive bands with different critical sequence length m and that of the toluene band.

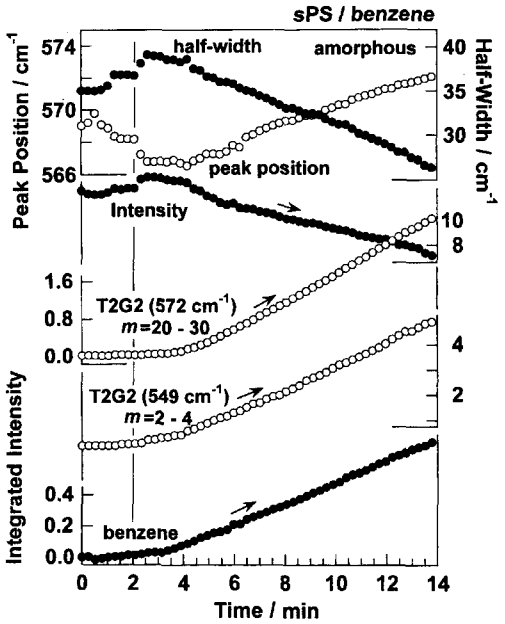

Figure 14. Time dependencies of the half-width, peak frequency, and integrated intensity of the 565 cm^{-1} amorphous band of the glassy sPS film measured in the process of benzene injection at room temperature, which are compared with the time dependencies of the integrated intensities of the crystalline-sensitive bands with different critical sequence length m and that of the benzene band.

stage of structural ordering, we noticed that the half-width of the amorphous bands began to decrease and the peak position shifted toward higher frequency side, quite contrast to the observation in the initial stage. These phenomena are considered to come from the reduction of the mobility of the amorphous chains which are constrained more or less in between the developed crystalline parts.

Conclusions

In this paper the structural changes occurring in the isothermal crystallization process of PE from the melt and the solvent-induced crystallization process of sPS glass were described by summarizing a series of our original papers. The molecular structural changes in these phenomena are quite complicated. Therefore we combined the various kinds of the techniques and, as a result, we could clarify these complicated structural changes from both the microscopic and the macroscopic points of view or from the different angles. Of course we have still many unresolved problems to reveal the essential features of the crystallization processes. We believe these studies will give us very important new ideas useful for the development of the novel polymer materials with systematically-controlled higher order structure and excellent physical properties.

Acknowledgements. The authors wish to thank professor Yoshinobu Izumi (Yamagata University), Dr. Katsumi Kobayashi (High Energy Accelerator Research Organization), Dr. Masayuki Imai (Ochanomizu Women's University), Dr. Yasuo Yamaguchi, Dr. Masayoshi Ohashi and Dr. Kenji Ohyama (Tohoku University) for their kind help in neutron and synchrotron experiments. They also wish to thank Toyobo Co., Ltd., Exxon Chemicals Co., Ltd., and Idemitsu Petrochemical Co., Ltd. for kindly supplying the ultra-drawn PE samples, linear low-density PE samples, and syndiotactic polystyrene, respectively.

References

(1) J. M. Schultz, *J. Polym. Sci., Polym. Phys. Ed.*, **14**, 2291 (1976).
(2) J. M. Schultz, J. S. Lin, and R. W. Hendricks, *J. Appl. Crystallogr.*, **11**, 551 (1978).
(3) G. Strobl and M. Schneider, *Macromolecules*, **18**, 1343 (1980).
(4) T. Albrecht and G. Strobl, *Macromolecules*, **28**, 5827 (1995).
(5) T. Albrecht and G. Strobl, *Macromolecules*, **29**, 783 (1996).
(6) P. J. Barham and A. Keller, *J. Polym. Sci., Polym. Phys. Ed.*, **27**, 1029 (1989).
(7) H. H. Song, R. S. Stein, D. Q. Wu, M. Ree, J. C. Phillips, A. LeGrand, and B. Chu, *Macromolecules*, **21**, 1180 (1988).
(8) H. H. Song, D. Q. Wu, B. Chu, M. Satkowski, M. Ree, R. S. Stein, and J. C. Phillips, *Macromolecules*, **23**, 2380 (1990).
(9) R. S. Stein, J. Cronauer, and H. G. Zachmann, *J. Molecular Structure*, **383**, 19 (1996).
(10) S. Rastogi, M. Hikosaka, H. Kawabata, and A. Keller, *Macromolecules*, **24**, 6384 (1991).
(11) M. Hikosaka, S. Rastogi, A. Keller, and H. Kawabata, *J. Macromol. Sci. Phys.*, **B31**, 87 (1992).
(12) S. Rastogi, *Prog. Colloid Polym. Sci.*, **87**, 42 (1992).
(13) K. Tashiro, S. Sasaki, and M. Kobayashi, *Polym. J.*, 1998, **30**, 485.
(14) S. Sasaki, K. Tashiro, M. Kobayashi1, Y. Izumi, and K. Kobayashi, *Polymer*, **40**, 7125 (1999).
(15) S. Sasaki, K. Tashiro, N. Gose, K. Imanishi, M. Izuchi, M. Kobayashi, M. Imai, M. Ohashi, Y. Yamaguchi, and K. Ohyama, *Polym. J.*, **31**, 677 (1999).
(16) D. C. Bassett, S. Block, and G. J. Piermarini, *J. Appl. Phys.*, **45**, 4146 (1974).
(17) M. Yasuniwa, M. Yamaguchi, A. Nakafuku, and A. Tsubakihara, *Polym. J.*, **22**, 411 (1990).
(18) A. J. Pennings and A. Zwijnenburg, *J. Polym. Sci., Ploym. Phys. Ed.*, **17**, 1011 (1979).
(19) J. Snook and A. J. Pennings, *Coll. Polym. Sci.*, **262**, 712 (1984).
(20) P. J. Lemstra, N. A. J. M. van Aerle, and C. W. M. Bastiaansen, *Polym. J.*, **19**, 85 (1987).
(21) H. Kyotani and Y. Tanabe, *Kobunshi Ronbunshu (Polymer Chemistry)*, **46**, 51 (1989).
(22) G. L. Liang, D. W. Noid, B. G. Sumpter, and B. Wunderlich, *J. Polym. Sci., Ploym. Phys. Ed.*, **31**, 1909 (1993).
(23) K. Tashiro, S. Sasaki, and M. Kobayashi, *Macromolecules*, **29**, 7460 (1996).
(24) B. Ewen, G. R. Strobl, and D. Richter, *J. Chem. Soc., Faraday Discuss.*, **69**, 19 (1980).
(25) Y. Kim, H. L. Strauss, and R. G. Snyder, *J. Phys. Chem.*, **93**, 7520 (1989).
(26) T. Hashimoto, T. Izumitani, and M. Takenaka, *Macromolecules*, **22**, 2293 (1989).

(27) K. Tashiro, *Acta Polymer.*, **46**, 100 (1995).
(28) Special issue on chain folding problem; *Faraday Discuss. Chem. Soc.*, 1979, **68**.
(29) Proceedings of the NATO Advanced Research Workshop on Crystallization of Polymers, Series C, M. Dasiere, Ed., Kluwer Academic Publishers, 1993, Vol. 405.
(30) Y. Chatani, Y. Shimane, Y. Inoue, T. Inagaki, T. Ijitsu, and T. Yukinari, *Polymer,* **33**, 488 (1992).
(31) Y. Chatani, Y. Shimane, T. Inagaki, T. Ijitsu, and T. Yukinari, *Polymer,* **34**, 1625 (1993).
(32) G. Guerra, V. Vincenzo, M. Vitagliano, C. De Rosa, V. Petraccone, and P. Corradini, *Macromolecules,* **23**, 1539 (1990).
(33) C. De Rosa, M. Rapacciuolo, G. Guerra, V. Petraccone, and P. Corradini, *Polymer,* **33**, 1423 (1992).
(34) Y. Chatani, Y. Shimane, T. Inagaki, T. Ijitsu, T. Yukinari, and H. Shikuma, *Polymer,* **34**, 1620 (1993).
(35) C. De Rosa, *Macromolecules,* **29**, 8460 (1996).
(36) P. Corradini, C. De Rosa, G. Guerra, R. Napolitano, V. Petraccone, and B. Porozzi, *Eur. Polym. J.,* **30**, 1173 (1994).
(37) M. Tosaka, N. Hamada, M.Tsuji, S. Kohjiya, T. Ogawa, S. Isoda, and T. Kobayashi, *Macromolecules,* **30**, 4132 (1997).
(38) N. Hamada, M. Tosaka, M. Tsuji, S. Kohjiya, and K. Katayama, *Macromolecules,* **30**, 6888 (1997).
(39) M. Tosaka, N. Hamada, M. Tsuji, and S. Kohjiya, *Macromolecules,* **30**, 6592 (1997).
(40) S. J. Spell, *Makromol. Symp.,* **114**, 63 (1997).
(41) C. De Rosa, G. Guerra, V. Petraccone, and P. Corradini, *Polym. J.* **23**, 1435 (1991).
(42) E. J. Kellar, C. Galiotis, and E. D. Andrews, *Macromolecules,* **29**, 3515 (1996).
(43) E. J. Kellar, A. M. Evans, J. Knowles, C. Galiotis, and E. D. Andrews, *Macromolecules,* **30**, 400 (1997).
(44) N. M. Reynolds and H. D. Stidham, and S. L. Hsu, *Macromolecules,* **24**, 3662 (1991).
(45) N. M. Reynolds and S. L. Hsu, *Macromolecules,* **23**, 3463 (1990).
(46) R. A. Nyquist, C. L. Putzig, M. A. Leugers, R. D. McLachlan, and B. Thill, *Appl. Spectrosc.,* **46**, 981 (1992).
(47) P. Musto, S. Tavone, G. Guerra, and C. De Rosa, *J. Polym. Sci., Polym. Phys.,* **35**, 1055 (1997).
(48) C. G. Zimba and J. F. Rabolt, *Macromolecules,* **22**, 2867 (1989).
(49) M. Kobayashi, T. Nakaoki, and N. Ishihara, *Macromolecules,* **22**, 4377 (1989).
(50) M. Kobayashi, T. Nakaoki, and N. Ishihara, *Macromolecules,* **23**, 78 (1990).
(51) K. Tashiro, Y. Ueno, A. Yoshioka, F. Kaneko, and M. Kobayashi, *Macromol. Symp.,* **141**, 33 (1999).
(52) K. Tashiro, A. Yoshioka, Y. Ueno, and M. Kobayashi, Proceedings of the 12th International Conference on Fourier Transform Spectroscopy (Au- gust 22-27, 1999, Tokyo, Japan).
(53) K. Tashiro and A. Yoshioka, *Polym. Prepr. Jpn.,* **48**, 3813 (1999).
(54) M. Kobayashi, K. Akita, and H. Tadokoro, *Die Makromol. Chem.,* **118**, 324 (1968).
(55) M. Kobayashi, *Makromol. Symp.,* **114**, 1 (1997).